

Towards Underwater Detection of Diluted Bitumen with Interdigital Sensors

Graziella Bedenik, Melissa Greeff, and Matthew Robertson
Queen's University, Kingston, Canada
{graziella.bedenik, melissa.greeff, m.robertson}@queensu.ca

Abstract—Diluted bitumen spills in freshwater environments pose significant challenges for detection and remediation due to the complex behaviour of the material once released, rendering traditional oil monitoring techniques, such as aerial surveys and fluorometry, ineffective. This study investigates the feasibility of utilizing interdigital capacitive sensors to detect dilbit in water via frequency-dependent impedance measurements. Three sensor designs were fabricated and tested with a vector network analyzer across samples with varying dilbit concentrations. All capacitor designs were able to detect electrical changes in water and exhibited different linear regions, suggesting a strong potential for quantitative sensing. These findings support the integration of the sensors into autonomous underwater robotic platforms for real-time, distributed monitoring of dilbit spills in freshwater systems.

Index Terms—interdigital sensors, capacitance measurement, dilbit, environmental monitoring, underwater sensing

I. INTRODUCTION

Freshwater ecosystems play a vital role in sustaining biodiversity, public health, and regional economies. In Canada, home to the world's largest surface freshwater reserves [1], these systems face increasing threats from anthropogenic stressors such as municipal and industrial pollution [2] and eutrophication-driven algal blooms [3]. Despite their ecological and economic significance, freshwater environments remain significantly under-researched compared to their terrestrial and marine counterparts [4].

Among the most complex pollutants affecting Canadian freshwater is diluted bitumen (dilbit), a heavy crude oil product transported across the country by rail and pipeline. Dilbit is produced by blending highly viscous bitumen with diluents to reduce viscosity for transport. In the event of a spill, the diluent quickly evaporates, leaving behind a dense, adhesive residue that can submerge or sink, making it difficult to detect, recover, or contain [5].

Existing techniques for oil detection in aquatic environments—such as aerial imaging, sonar, fluorometry, and diver observations—are limited in their effectiveness for submerged or weathered dilbit [5], [6]. These methods are often expensive, sensitive to environmental conditions, and lack continuous or distributed monitoring capabilities. Fluorometry, although widely used for oil detection, has

shown inconsistent results when applied to weathered or sunken dilbit [7]. This motivates the development of new sensing systems that are robust, embeddable, cost-effective, and capable of operating in real time.

Subaquatic robots have emerged as promising platforms for environmental monitoring [8], [9], with growing interest in their use by Canadian institutions [10], [11]. However, while robotic platforms for freshwater monitoring have been proposed [11], the integration of suitable sensors remains an open challenge. For example, electrochemical sensors have shown promising results for pollutant detection in marine environments [12], and capacitive sensors have been used for estimating oil film thickness in marine surface spills [13]–[15].

Despite growing evidence that changes in the electrical properties of water can indicate the presence of hydrocarbons, several instrumentation-relevant aspects remain underexplored, especially for dilbit. Prior studies have not examined the frequency-dependent behaviour of electrical properties, nor compared which electrical quantities (e.g., conductance, capacitance, or impedance) are most selective or practical for embedded sensing. Additionally, there is a lack of experimental work on the electrical signature of dilbit in water, particularly in forms compatible with robotic integration.

This study addresses these gaps by investigating the use of interdigital capacitive sensors for detecting dilbit in freshwater environments. Owing to their planar geometry and compatibility with embedded systems, interdigital sensors are particularly well-suited for integration into mobile robotic platforms. The sensors were designed to operate in the high-frequency regime, where capacitive effects are dominant and less susceptible to electrolysis or electrical noise. Water-accommodated fraction (WAF) samples with varying dilbit concentrations were prepared and analyzed using a vector network analyzer (VNA), enabling the identification of frequency ranges with maximum sensitivity. The main contributions of this work include a frequency-dependent impedance analysis of interdigital capacitive sensors exposed to dilbit-contaminated water; the identification of the best operating regions for quantitative detection based on imaginary impedance variation; a comparative evaluation of three sensor geometries in terms of sensitivity and linearity range; and practical insights into sensor integration strategies for future deployment in autonomous freshwater monitoring robots.

We acknowledge the support of the Natural Sciences and Engineering Research Council of Canada (NSERC) [funding reference number RGPIN-2021-04049] and the Ingenuity Labs Research Institute for partially funding this research.

II. SENSOR DESIGN AND FABRICATION

This study investigates the performance of custom-designed interdigital capacitive sensors for detecting varying concentrations of dilbit WAFs in distilled water. These sensors feature an interdigitated electrode structure—two sets of parallel electrodes arranged in an alternating planar configuration, as shown in Fig. 1. Depending on the operating frequency, each digit interacts with the surrounding medium in distinct ways, influencing the sensor’s impedance response [16]. The primary sensing principle relies on measuring impedance variations induced by changes in material properties, such as the presence and concentration of a target chemical.

Because dilbit contamination alters the electrical properties of water, particularly effective permittivity and conductivity, capacitive sensing offers a promising approach for concentration discrimination. Establishing a clear relationship between these parameters and sensor response is essential for developing a sensing strategy compatible with aquatic robotic platforms for real-time environmental monitoring. This section describes the rationale behind the sensor selection, as well as the design geometry and fabrication of the three custom interdigital sensors used in this work.

A. Rationale for Interdigital Sensor Selection

Among capacitive sensing architectures, planar interdigital designs were selected due to their compact geometry, single-sided measurement capability, and ease of integration into robotic systems. Unlike parallel-plate capacitors, which offer higher nominal capacitance but pose significant challenges for underwater integration, interdigital sensors provide a planar layout that simplifies waterproofing and mounting onto curved or confined surfaces. The ability to tailor electrode layout to shape the electric field distribution is particularly advantageous for embedded sensing applications.

Despite their benefits, planar designs typically exhibit lower capacitance values and are more prone to parasitic effects, especially inductance from long electrode fingers. To mitigate these drawbacks, design choices included limiting digit length to reduce inductive effects and opting for impedance-based sensing at high frequencies. Direct capacitance measurement at low frequencies or DC was avoided due to risks of electrolysis and a poor signal-to-noise ratio in the picofarad range.

To address the limited absolute capacitance and enhance discrimination capabilities, a VNA was used to characterize sensor impedance across a broad frequency sweep. This approach enables the identification of frequency bands where capacitive responses are both stable and sensitive to WAF concentration, thus improving measurement robustness and providing a viable strategy for integration into autonomous robotic systems.

B. Design Methodology and Fabrication

Two main aspects informed the design of the three interdigital sensor designs ($x = 1, 2, 3$): (1) the geometric

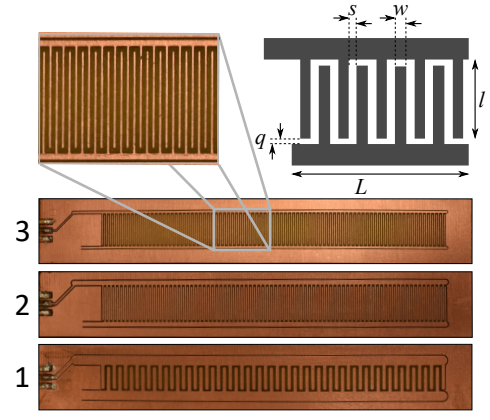


Fig. 1: The manufactured interdigital sensors, with a zoomed-in view of the digit resolution for design 3. At the upper right corner, a simplified interdigital sensor and its design parameters are shown. Adapted from [16].

constraints imposed by the test setup, and (2) the theoretical relationship governing capacitance in interdigital structures. The capacitance of the interdigital structure was estimated using the analytical model [17]

$$C[\text{pF}] = 10^{-3} \cdot \frac{\epsilon_r}{18\pi} \cdot \frac{K(k)}{K'(k)} \cdot l \cdot (N - 1), \quad (1)$$

where l is in microns, N is the number of digits, and ϵ_r is the effective dielectric constant. The ratio $\frac{K(k)}{K'(k)}$ accounts for fringing fields and depends on the geometry, using the parameters shown in Fig. 1.

The sensors were designed to fit vertically into standard 25 mm \times 150 mm test tubes, constraining the PCB footprint to 21.5 mm \times 135 mm. A fixed active length $L = 105$ mm and $q = 0.5$ mm were shared across all designs for consistency. A sensitivity analysis varying N , w , s , and l by $\pm 10\%$ showed N and l had the strongest influence on total capacitance. These were thus prioritized for variation across sensor designs.

Using (1) and the known geometric constraints, we estimated the relative capacitance of each sensor design. Design 2, which had 164 digits each measuring 11,000 μm in length and spaced 140 μm apart, exhibited the highest estimated capacitance. Design 3 followed closely, with 170 digits of 10,000 μm length and 425 μm spacing. Design 1, with only 59 digits of 7,500 μm length and 850 μm spacing, resulted in the lowest capacitance. As expected, sensors with a greater number of longer and more closely spaced digits achieved higher capacitance, providing an early indication of their relative sensitivity in capacitive sensing applications.

The sensors, displayed in Fig. 1, were fabricated on FR4 substrate using a CNC milling machine (ProtoMat S64, LPKF Laser & Electronics, Germany). Post-fabrication, the copper layer was cleaned using steel wool and isopropyl alcohol and inspected for continuity. SMA connectors were soldered, and the boards were coated with a conformal acrylic layer (419D-340G, MG Chemicals Ltd, Canada) to electrically insulate the traces and prevent corrosion.

III. METHODS

To evaluate the performance of the fabricated interdigital sensors in detecting varying concentrations of dilbit WAFs, we conducted a series of controlled laboratory experiments. A WAF is a laboratory-prepared medium that represents the fraction of a substance (like an oil) that dissolves or disperses in water. It's essentially an aqueous solution containing dissolved components of a complex substance, often used for toxicity testing or analysis. WAFs help to account for solubility differences within a complex substance, allowing for a more accurate representation of the substance's effects in an aquatic environment. WAF preparation and testing have been widely used in environmental science and regulatory contexts, particularly for petroleum products [18]. Given these advantages, WAFs were used as the medium for characterizing sensor performance across known dilbit concentrations, enabling controlled, repeatable analysis of the sensor's impedance response.

The procedures focused on two main components: the preparation of repeatable, well-characterized WAF samples across a defined concentration range, and the acquisition of impedance data under consistent conditions using a VNA. The methods described in subsections III-A and III-B detail the protocols for sample preparation and sensor testing, respectively.

A. Sample Preparation

Sample preparation followed a small-volume protocol adapted from Adams et al. [19], which was adapted from the gold standard in the field, published by Aurand and Coelho for the American Petroleum Institute in 2005 [18]. Fresh Cold Lake Blend dilbit, poured on February 3rd, 2025, was stored sealed and refrigerated until use on May 22nd, 2025.

Eleven dilutions, ranging from 0% to 100% WAF in 10% increments, were prepared using distilled water and poured into labelled 25 mm × 150 mm glass test tubes. Each tube was filled to 50 mL to maintain the recommended 20–30% headspace. The same guideline was applied to the mixing container. All procedures were performed in a fume hood due to dilbit's toxicity, and ambient temperature was monitored using a pre-calibrated DS18B20 sensor connected to an Arduino Uno and a real-time clock shield.

All glassware was initially rinsed with water, dried, and then cleaned with isopropyl alcohol. For each capacitor design described in section II, the following steps were performed: 720 mL of distilled water was added to a 1 L glass beaker along with a 25 mm magnetic stir bar, and mixed at 220 rpm (adjusted to prevent vortex formation). Temperature monitoring began, and 80 mL of dilbit was gently added to the centre of the beaker. The beaker was then covered with aluminum foil, and the mixture was stirred continuously for 18 hours to form the WAF. To prepare dilutions, test tubes were pre-filled with specific volumes of distilled water (0–50 mL, in 5 mL increments). The surface oil was gently pushed aside using a scoopula, and the

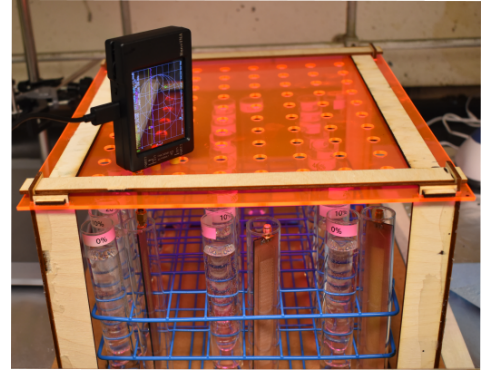


Fig. 2: Perspective view of the test tube rack positioned within the custom alignment apparatus.

aqueous phase was extracted using a 22-gauge gastight syringe (1000 Series, Hamilton Company, USA), then transferred to the corresponding test tube to complete the desired dilution.

B. Experimental Setup and Methods

Once all the test tubes were filled with the designated WAF concentrations, each test tube was randomly assigned one of the 33 fabricated sensors to assess impedance response across concentrations. Before immersion, ten S_{11} acquisitions were recorded in air for each sensor design as a reference, as shown in Fig. 2. During experiments, sensors were fully immersed in the liquid sample, and measurements were taken using a handheld VNA (nanoVNA-H v1.2.27). The device was calibrated between 100 kHz and 300 MHz with 3201 data points, and ten acquisitions were recorded per sample using the NanoVNA-App (v1.1.208, OneOfEleven).

The S_{11} parameter, also known as the input reflection coefficient or return loss, reflects the amount of power reflected to the source due to impedance mismatch. A value of $S_{11} = 0$ dB indicates total reflection, whereas more negative values (e.g., $S_{11} = -10$ dB) correspond to better matching and partial absorption. In our case, S_{11} data were used to extract the complex impedance (Z) of each sensor via the standard transformation

$$Z = Z_0 \frac{1 - \Gamma}{1 + \Gamma}, \quad (2)$$

where the complex reflection coefficient $\Gamma = \text{Re}(S_{11}) + j\text{Im}(S_{11})$ incorporates both measured components of the reflection coefficient and $Z_0 = 50 \Omega$.

To reduce variability and ensure repeatability, several setup controls were implemented. Within four hours of making the WAF mixture, the same person prepared all samples with the same WAF and distilled water sources. A custom fixture aligned each test tube relative to the VNA, and the same coaxial cable, cut to a fixed length and orientation, was used throughout. Sensor handling and positioning were performed consistently by a single operator, who remained in the same spot for all acquisitions.

IV. RESULTS AND DISCUSSION

This section presents the electrical characterization of the three interdigital sensor designs ($x = 1, 2, 3$) when exposed to varying concentrations of dilbit WAFs. The analysis focuses on interpreting the impedance data obtained from S_{11} measurements, with the aim of informing sensor selection and usage. The temperature inside the fume hood during both sample preparation and experiments was kept around 18 °C.

Due to significant measurement instability observed at very low frequencies, the range below 500 kHz was excluded from analysis. Although the nanoVNA performs reliably from approximately 500 kHz and above, the frequency window between 500 kHz and 50 MHz was found to contain no additional information relevant to the discrimination of dilbit concentrations. Consequently, the analysis presented in this study focuses on the 50 MHz to 300 MHz range, where the sensor response exhibited clearer and more consistent behaviour, as indicated by Fig. 3.

All results presented in this study are based on the average of ten repeated acquisitions per sample. The standard deviation values across these acquisitions were consistently low, indicating strong measurement repeatability. For the real part of the impedance $\text{Re}(Z)$, median standard deviations were below 0.014 Ω for all capacitor designs, with maximum values of 6.14 Ω , 2.90 Ω , and 7.35 Ω for designs 1, 2, and 3, respectively. The imaginary part $\text{Im}(Z)$ showed negligible variation, with all standard deviations effectively zero across all measurements.

A. Interpreting Real and Imaginary Impedance Components

Upon examining the real part of the impedance ($\text{Re}(Z)$), i.e., resistance, variations were observed across WAF concentrations, as shown by the top graphs in Fig. 3 and Fig. 4. In the latter, the curves shown refer to capacitor 2 and a reduced frequency range, which facilitates visualization of the phenomenon that repeats throughout the analyzed frequency range. Relatively similar behaviours were observed for capacitors 1 and 3, with the choice of showing only one design being motivated purely by the succinctness of the text.

Ideally, $\text{Re}(Z)$ should remain negligible if the system behaved as a purely capacitive interface. However, the copper

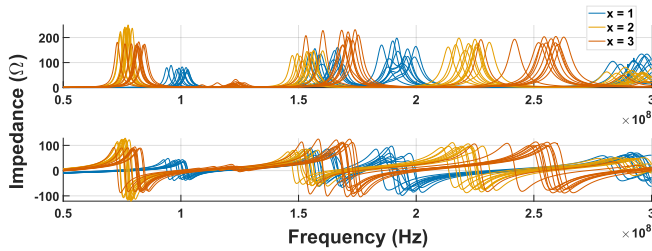


Fig. 3: Impedance (Z) information recovered from the measured S_{11} parameter for all evaluated concentrations by all capacitor designs in the full studied range. Top: real part of Z and bottom: imaginary part of Z .

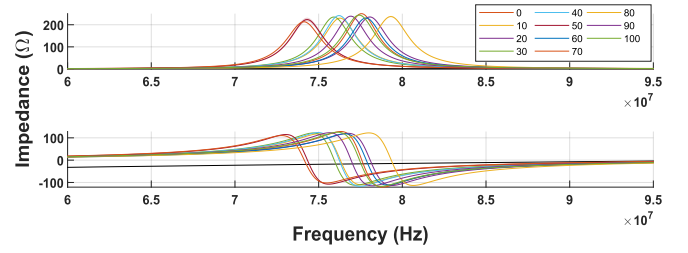


Fig. 4: Impedance (Z) information recovered from the measured S_{11} parameter for all evaluated concentrations by capacitor design 2 between 60 MHz and 95 MHz. Top: real part of Z and bottom: imaginary part of Z .

layer resistance exhibits a strong frequency dependence due to the skin effect [20], a phenomenon particularly relevant in high-frequency systems, such as our sensors. The inverse of resistance is conductance, a widely used physical property of materials that helps identify, classify, or quantify them. Conductance can therefore be a characteristic of interest for measurement in our application. However, from a sensing perspective, in addition to being less selective, the circuits that measure conductance in situ are usually more complex, since they generally convert resistance information to voltage and then modulate it for transmission. When measuring capacitance or inductance, in addition to being more selective, the response can be more easily obtained in frequency, eliminating the need for modulation.

Given these trade-offs, this study focused on the imaginary part of the impedance ($\text{Im}(Z)$). Analysis of $\text{Im}(Z)$ across frequencies confirms that each sensor exhibits a transition between capacitive (negative $\text{Im}(Z)$) and inductive (positive $\text{Im}(Z)$) behaviour, as highlighted by the bottom graphs in Fig. 3 and Fig. 4. As expected from the electrode geometry, this transition is frequency-dependent and varies with WAF concentration. Inductive effects tend to dominate at higher frequencies, especially in structures with long, narrow conductive paths, such as interdigital fingers. These effects must be carefully managed in subaquatic environments, where proximity to surrounding objects, particularly those with higher magnetic permeability, can significantly influence inductive behaviour. For this reason, the analysis prioritizes frequency regions where $\text{Im}(Z)$ remains negative, corresponding to a dominantly capacitive response that is more stable and suitable for concentration discrimination.

The desired operation occurs in the frequency range where the vertical separation between curves representing different WAF concentrations is maximized. These regions allow for more distinguishable responses, aiding in the estimation of concentration. However, measurements near the resonance transition should be avoided due to high instability between inductive and capacitive responses.

Beyond these initial observations, two additional noteworthy but unexplained phenomena were identified. First, by examining the overlapping of $\text{Re}(Z)$ and $\text{Im}(Z)$ in Fig. 4, it can be seen that $\text{Re}(Z)$ tends to peak at frequencies where $\text{Im}(Z) = 0$, then dampens before rising

again near subsequent resonance points. These turning frequencies also shift with concentration. This sensitivity to dilbit concentration implies that the zero-crossing frequency itself could serve as an additional measurement feature in future sensing strategies. Second, there are several frequency points where two different concentrations yield the same impedance magnitude for a given sensor. This ambiguity suggests that a thresholding strategy or restricted frequency band selection must be defined for practical deployment to avoid misclassification.

B. Capacitive Impedance Analysis and Optimal Frequency Selection

To analyze the capacitive behaviour of each sensor, a frequency was considered to be within the capacitive region if $\text{Im}(Z) \leq 0$ for all concentrations at that point. Within these regions, the range of $\text{Im}(Z)$ values across concentrations was computed as a function of frequency to identify points where the sensor exhibited the greatest sensitivity. For capacitor 1, the maximum variation was 74.45Ω at 199.80 MHz . Capacitor 2 showed the largest response variation, 105.11Ω , occurring at 79.39 MHz . Capacitor 3 exhibited a similar performance, with a peak variation of 104.30Ω at 176.38 MHz .

To determine the most suitable frequency for concentration discrimination within the capacitive regime, a scoring approach was implemented. For each capacitor design, all frequencies where the imaginary part of the impedance satisfied $\text{Im}(Z) \leq 0$ across all WAF concentrations were identified as valid candidates. At each of these frequencies, a score was computed using

$$\text{Score}(f) = d_f + \alpha \cdot \Delta \text{Im}(Z)_f, \quad (3)$$

where d_f is the distance (in MHz) from frequency f to the nearest zero-crossing of $\text{Im}(Z)$ (i.e., where it becomes positive for any concentration), $\Delta \text{Im}(Z)_f$ is the range of imaginary impedance values across all concentrations at that frequency, and $\alpha = 0.001$ is a scaling factor used to adjust

the influence of the impedance range. This formulation emphasizes frequency stability while still accounting for sensitivity.

The frequency with the highest score was selected as the optimal operating point for each sensor design. The resulting selection is shown in Table I. For capacitors 2 and 3, the frequencies obtained through this analysis were the same where the impedance variation had already reached its maximum.

TABLE I: Best Frequency and Corresponding Impedance Variation for Each Capacitor Design

x	Best Frequency (MHz)	Variation (Ω)
1	204.13	55.52
2	79.39	105.11
3	176.38	104.30

Finally, the $\text{Im}(Z)$ values at the found capacitive frequencies were plotted as a function of concentration for each capacitor design, as shown in Fig. 5. These curves reflect the sensitivity of each design to changes in concentration and were used to assess the potential linearity of the sensor response.

Analyzing this data reveals that not only do different dilbit concentrations alter key electrical properties of water, but also that capacitive sensors are sensitive to such changes, highlighting their potential in detecting and distinguishing between concentrations. Based on the impedance range data at optimal frequencies, the sensors demonstrated discernible responses to concentration differences as small as 10% WAF. This suggests that, even in their preliminary form, the sensors can reliably distinguish between modest concentration shifts—a critical capability for detecting the onset and spread of diluted bitumen contamination.

Nonetheless, as seen in Table I, capacitor designs $x = 2$ and $x = 3$ exhibited more prominent variation with concentration than $x = 1$. However, each sensor design showcases a range of four analyzed concentrations where the behaviour is linear, as indicated by the dashed rectangles in Fig. 5. From a sensing perspective, linear behaviour is desirable due to simplified calibration, better measurement precision, and ease of predictability in system behaviour.

Capacitor 2 demonstrated the highest variation in impedance across concentrations (105.11Ω) and maintained a clear linear region within a mid-range concentration window (20–50% WAF). This makes it the most promising candidate for general-purpose sensing, especially in early spill detection scenarios. Capacitor 3, while nearly matching capacitor 2 in terms of impedance range (104.30Ω), exhibited linearity at lower concentrations, which could be beneficial for the detection of more diluted or dispersed dilbit. Capacitor 1, although exhibiting the lowest sensitivity and more limited linearity, showed consistent behaviour at higher concentrations, suggesting potential utility in detecting denser accumulations or proximity to the spill source.

These findings suggest that no single design is universally optimal. Instead, a multi-sensor approach, either as an array embedded in a single platform or distributed among

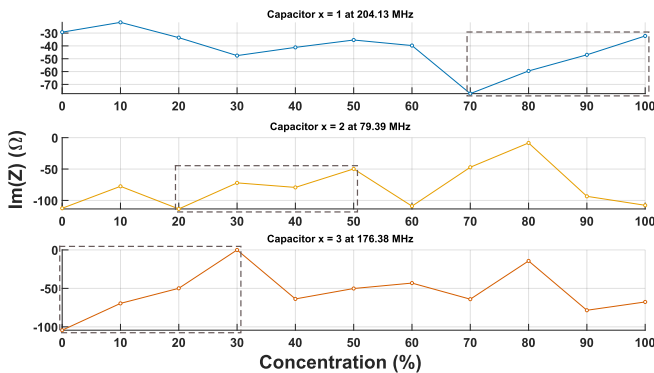


Fig. 5: Imaginary impedance measurements for each concentration taken at the frequency where the capacitor displays the greatest sensitivity. From top to bottom: capacitor 1 at 204.13 MHz , capacitor 2 at 79.39 MHz , and capacitor 3 at 176.38 MHz . The dashed rectangles indicate regions where the sensor response is linear for four consecutive analyzed concentrations.

specialized robotic agents, may enhance overall monitoring performance. Besides, for real-world deployment, environmental robustness must be considered. While the controlled lab conditions ensured stable measurements, factors such as temperature variation, ionic content, and water flow may affect impedance readings in situ. Future work should therefore include validation in simulated natural environments and robustness testing under expected operational conditions.

V. CONCLUSION

This study investigated the feasibility of using interdigital capacitive sensors for the underwater detection of dilbit in freshwater environments. By analyzing the impedance response of three different sensor designs across a range of known WAF concentrations, we demonstrated that variations in the electrical properties of the medium, particularly in the capacitive regime, can be effectively captured and used for concentration discrimination in the case of fresh Cold Lake Blend dilbit.

We found that it is possible to measure a small linear range of lower, mid-range, or upper concentration levels by tuning the sensor design. The complementary characteristics of each sensor in terms of sensitivity and linear measurement region suggest that a multi-sensor or distributed deployment strategy may improve the spatial and quantitative resolution of dilbit spill detection.

Impedance measurements focused primarily on the capacitive part of the imaginary component ($\text{Im}(Z)$). This choice not only enhances selectivity but also facilitates sensor integration into frequency-based readout circuits, an essential consideration for robotic deployment. Such platforms could enable real-time, distributed monitoring of freshwater ecosystems, improving early spill detection and response, and potentially providing actionable data to enhance the assessment and management of freshwater ecosystems, ultimately contributing to environmental conservation.

Future work will focus on investigating other types and weathering conditions of dilbit, in situ validation, environmental robustness, and the integration of signal processing frameworks to support adaptive sensing and autonomous decision-making.

ACKNOWLEDGEMENT

We thank Dr. Bruce Hollebone (Environment and Climate Change Canada) for facilitating access to diluted bitumen, Dr. Julie Adams for guiding sample preparation protocols, and Diancheng Li for assisting with sensor manufacturing. We also thank Dr. Xian Wang for providing access to the fume hood and other laboratory resources necessary for conducting the experiments and Dr. Elyson Carvalho for the invaluable discussions and insights provided.

REFERENCES

- [1] S. Stoyanovich, Z. Yang, M. Hanson, B. Hollebone, D. M. Orihel, V. Palace, J. Rodriguez-Gil, F. Mirnaghi, K. Shah, and J. Blais, "Fate of polycyclic aromatic compounds from diluted bitumen spilled into freshwater limnocostracans," *Science of The Total Environment*, vol. 819, p. 151993, 2022.
- [2] C. Rolsky, V. Kelkar, E. Driver, and R. U. Halden, "Municipal sewage sludge as a source of microplastics in the environment," *Current Opinion in Environmental Science & Health*, vol. 14, pp. 16–22, 2020.
- [3] C. Binding, L. Pizzolato, and C. Zeng, "Eolakewatch; delivering a comprehensive suite of remote sensing algal bloom indices for enhanced monitoring of canadian eutrophic lakes," *Ecological Indicators*, vol. 121, p. 106999, 2021.
- [4] G. Su, M. Logez, J. Xu, S. Tao, S. Villéger, and S. Brosse, "Human impacts on global freshwater fish biodiversity," *Science*, vol. 371, no. 6531, pp. 835–838, 2021.
- [5] N. A. of Sciences, D. on Earth, L. Studies, B. on Chemical Sciences, and C. on the Effects of Diluted Bitumen on the Environment, *Spills of diluted bitumen from pipelines: A comparative study of environmental fate, effects, and response*. National Academies Press, 2016.
- [6] M. Fingas, "Diluted bitumen (dilbit): A future high risk spilled material," *Proceedings of Interspill*, p. 24, 2015.
- [7] W. Ji, A. G. Slaughter, G. M. Coelho, T. J. Nedwed, R. C. Prince, and M. C. Boufadel, "Optimized underwater detection of dispersed oils using scanning fluorometry," in *International Oil Spill Conference Proceedings*, vol. 2024, no. 1. Allen Press, 2024.
- [8] M. Dunbabin and L. Marques, "Robots for environmental monitoring: Significant advancements and applications," *IEEE Robotics & Automation Magazine*, vol. 19, no. 1, pp. 24–39, 2012.
- [9] R. Bogue, "The role of robots in environmental monitoring," *Industrial Robot: the international journal of robotics research and application*, vol. 50, no. 3, pp. 369–375, 2023.
- [10] J. Lindsay, J. Ross, M. L. Seto, E. Gregson, A. Moore, J. Patel, and R. Bauer, "Collaboration of heterogeneous marine robots toward multidomain sensing and situational awareness on partially submerged targets," *IEEE Journal of Oceanic Engineering*, vol. 47, no. 4, pp. 880–894, 2022.
- [11] G. Bedenik, A. Morales, S. Pieris, B. da Silva, J. W. Kurelek, M. Greeff, and M. Robertson, "Bistable sma-driven engine for pulse-jet locomotion in soft aquatic robots," *arXiv preprint arXiv:2504.03988*, 2025.
- [12] S. K. Haghighi, S. Mohammadlou, S. Angizi, and A. Hatamie, "Innovative electrochemical nano-robot: Integrating printed nanoelectronics with a remote-controlled robotic for on-site underwater electroanalysis," *Langmuir: the ACS journal of surfaces and colloids*, vol. 41, no. 13, pp. 8592–8601, 2025.
- [13] M. Saleh, G. Oueidat, I. H. Elhadj, and D. Asmar, "In situ measurement of oil slick thickness," *IEEE Transactions on Instrumentation and Measurement*, vol. 68, no. 7, pp. 2635–2647, 2018.
- [14] M. Saleh, A. R. Tabikh, I. H. Elhadj, K. McKinney, and D. Asmar, "Dual-modality capacitive-ultrasonic sensing for measuring floating oil spill thickness," *IEEE Transactions on Instrumentation and Measurement*, vol. 71, pp. 1–14, 2022.
- [15] M. Saleh, I. H. Elhadj, and D. Asmar, "In situ sensors for oil spill detection and thickness measurement: Methods and challenges," *IEEE Transactions on Instrumentation and Measurement*, 2024.
- [16] H.-N. L. Teodorescu, "Constraints on planar and planar interdigital capacitors used in sensors," in *2024 16th International Conference on Electronics, Computers and Artificial Intelligence (ECAI)*. IEEE, 2024, pp. 1–6.
- [17] I. J. Bahl, *Lumped elements for RF and microwave circuits*. Artech house, 2022.
- [18] D. Aurand and G. Coelho, "Cooperative aquatic toxicity testing of dispersed oil and the chemical response to oil spills: Ecological effects research forum (croserf)," *Inc. Lusby, MD. Tech. Report*, pp. 07–03, 2005.
- [19] J. E. Adams, B. N. Madison, K. Charbonneau, M. Sereneo, L. Baillon, V. S. Langlois, R. S. Brown, and P. V. Hodson, "Effects on trout alevins of chronic exposures to chemically dispersed access western blend and cold lake blend diluted bitumens," *Environmental Toxicology and Chemistry*, vol. 39, no. 8, pp. 1620–1633, 2020.
- [20] S. Ramo, J. R. Whinnery, and T. Van Duzer, *Fields and waves in communication electronics*. John Wiley & Sons, 1994.